A Genome-Scale Modeling Approach to Quantify Biofilm Component Growth of *Salmonella Typhimurium*

Nicholas Ribaudo, Xianhua Li, Brett Davis, Thomas K. Wood, and Zuyi (Jacky) Huang

Abstract: *Salmonella typhimurium* (*S. typhimurium*) is an extremely dangerous foodborne bacterium that infects both animal and human subjects, causing fatal diseases around the world. Salmonella's robust virulence, antibiotic-resistant nature, and capacity to survive under harsh conditions are largely due to its ability to form resilient biofilms. Multiple genome-scale metabolic models have been developed to study the complex and diverse nature of this organism's metabolism; however, none of these models fully integrated the reactions and mechanisms required to study the influence of biofilm formation. This work developed a systems-level approach to study the adjustment of intracellular metabolism of *S. typhimurium* during biofilm formation. The most advanced metabolic reconstruction currently available, STM_v1.0, was 1st extended to include the formation of the extracellular biofilm matrix. Flux balance analysis was then employed to study the influence of biofilm formation on cellular growth rate and the production rates of biofilm components. With biofilm formation present, biomass growth was examined under nutrient rich and nutrient deficient conditions, resulting in overall growth rates of 0.8675 and 0.6238 h^{-1} respectively. Investigation of intracellular flux variation during biofilm formation resulted in the elucidation of 32 crucial reactions, and associated genes, whose fluxes most significantly adapt during the physiological response. Experimental data were found in the literature to validate the importance of these genes for the biofilm formation of *S. typhimurium*. This preliminary investigation on the adjustment of intracellular metabolism of *S. typhimurium* during biofilm formation will serve as a platform to generate hypotheses for further experimental study on the biofilm formation of this virulent bacterium.

Keywords: biofilm formation, genome-scale metabolic model, *Salmonella Typhimurium*

Practical Application: Salmonella is most commonly a foodborne pathogen that causes human diseases. It survives in the hostile environmental by forming biofilms. This work presents the 1st systems-level investigation of the intracellular metabolic adaptation of this pathogen during the biofilm formation. The metabolic reactions identified in this work for their important role in Salmonella biofilm formation can be further used as the targets for optimizing antibiotic selection to combat Salmonella biofilm.

Introduction

Pathogenic bacteria are a serious human health threat around the world; hence, they are widely studied to better combat human infection. Simple antibiotics were a primary defense, but unfortunately, the evolution of such bacteria to resist these antibiotics has resulted in the resurfacing of an old threat, untreatable bacterial infection (Björkman and others 1998). *Salmonella enterica* is one of the most commonly studied human pathogens due to its innate virulence, impact on society, and well-studied metabolic pathways (Kolter and Greenberg 2006; Thiele and others 2011). Salmonellais most commonly a foodborne pathogen, but has also created infectious threats through various surface interactions such as on medical devices (Gibson 2000; Kolter and Greenberg 2006). It infects both animal and human subjects, causing diseases such as typhoid, gastroenteritis, bacteremia, and many more infectious ailments (Jun 2006). In the United States alone, more than 500 human deaths occur annually due to infection by various strains of Salmonella, 95% of which are due to foodborne contamination (Mead and others 1999). The impact and severity of this pathogen is even greater in developing countries where sterility in the food industry is weaker. Salmonella contamination in food products primarily takes place through its attachment, survival, and proliferation on surfaces within food production facilities.

Salmonella's ability to survive under varying environmental conditions, resist antibiotic influence, and remain virulent is largely due to its ability to form resilient biofilms (Bower 1999; Stepanović and others 2004). Biofilms are multicellular populations of microorganisms that are connected through extracellular polymeric substances (EPSs), which provide the structural support for bacterial survival, proliferation, and virulence (Stoodley and others 2002). The structuralimplication of biofilm formation is far from the only impact that biofilms have on cell viability. The protective layer contributes to sophisticated cell–cell signaling that allows for defense mechanisms when the microbial communities are under stress, therefore stimulating survival (Gibson 2000; Stoodley and others 2002). A number of cells lay dormant in the biofilm community, protected by their extracellular matrix, allowing for enhanced protection against infection or environmental stress (Fux and others 2005). Although a large number of cells can be eliminated under such stresses, these dormant cells are less affected since antimicrobials primarily have been designed to eliminate

JFDS-2016-1280 Submitted 8/10/2016, Accepted 10/24/2016. *Authors Ribaudo, Li, Davis, and Huang are with Dept. of Chemical Engineering, Villanova Univ., Villanova 19085, PA, U.S.A. Author Wood is with Depts. of Chemical Engineering and Biochemistry and Molecular Biology, Pennsylvania State Univ., Univ. Park 16802, PA, U.S.A. Direct inquiries to author Huang (E-mail: zuyi.huang@villanova.edu).*

doi: 10.1111/1750-3841.13565

Journal of Food Science A Publication of the Institute of Food Technologists

metabolically active bacteria. Their survival allows for further proliferation and regeneration of their cellular community held together by the biofilm (Kell and others 2015). Such mechanisms are primary contributors to the evolution of antibiotic resistance and overall survival.

Salmonella's bacterial biofilms are capable of forming on animal surfaces and tissues, sediments and soils, as well as plastic, steel, glass, and a variety of other abiotic surfaces (Romling and others 1998; Gibson 2000; Solano and others 2002). This versatility of biofilm formation is due to the microorganism's ability to produce varying biofilms that exhibit diversity in structure, composition, and metabolic responses under diverse environmental conditions (Solano and others 2002; Kolter and Greenberg 2006; Kim and others 2013). The exceptional diversity of their formation and function makes studying biofilms in nature very difficult (Beloin and Ghigo 2005).

To better combat the complexity and diverse nature of metabolic pathways, such as those involved in the formation of biofilms, a genome-scale metabolic modeling approach can be employed. The applications of such modeling approaches have significantly influenced the ability to accomplish high-throughput analysis of metabolic networks (Kim and others 2012). Computerized reconstructions of genome-scale metabolic networks in MATLAB provide a platform to perform *in silico* simulations that elucidate the mechanistic relationship between genotype and phenotype. In other words, conducting studies of cellular metabolism at the genome level leads to a better understanding of phenotypic variation. Genome-scale models are used to accurately predict metabolic trends and draw important conclusions on cellular facets such as gene knockout results, optimal growth patterns, substrate preferences, changes in gene expression profiles, and shifts in intracellular metabolic fluxes under varying conditions (Price and others 2003). Understanding these aspects of cellular metabolism, and the detailed mechanisms behind them, provides an opportunity to better combat human diseases, virulent bacteria, and other infectious microorganisms (Butcher and others 2004; Kim and others 2012; Mardinoglu and others 2013). There are currently over 150 predictive metabolic network reconstructions available, spanning both prokaryotic and eukaryotic organisms (Feist and others 2008). These genome-scale metabolic models are currently being employed in the development of novel drugs to fight infections without consequential side effects. Calculated metabolic responses help to prioritize drug targets and design effective clinical trials (Butcher and others 2004). Genome-scale metabolic modeling approaches were developed to study microbial biofilm formation since 2012. In particular, Sigurdsson and others 2012 performed flux balance analysis (FBA) in a genome-scale model of *Pseudomonas aeruginosa* and predicted the microbial growth in the biofilm nutrient environment. The trend for biofilm formation, however, was not predicted in this paper. In order to address this issue, our group developed a systems-biology approach to indicate the trend of biofilm formation of *P. aeruginosa* when single genes were inhibited (Xu and others 2013) and under various environmental conditions (Xu and others 2015). In particular, the change of intracellular fluxes in the genome-scale model was used to indicate the trend of biofilm formation. Vital-Lopez and others 2015 presented a similar approach but used the change in the metabolite concentrations to indicate the biofilm formation of *P. aeruginosa*. Chen and others 2016 presented another model for solving biofilm process of *P. aeruginosa* in both time and spatial aspect, with indications of biomass and metabolic byproducts change. Other studies are either focused on capturing the spatial heterogeneity of microbial community in a biofilm (Mazumdar and others 2013) or solving the interaction of biofilm with extracellular components (Jayasinghe and others 2014). In the aforementioned approaches, no reaction was included for the production rates of biofilm components such as exopolysaccharide, lipopolysaccharide (LPS), and enterobacterial common antigen (ECA). The biofilm formation rate was thus not directly predicted from these approaches, although some indirect indications such as the change in metabolic fluxes or metabolite concentrations were used to monitor biofilm formation. In order to address this issue, biofilm formation reactions were integrated with a genome-scale model for the 1st time in this work to study the biofilm formation of the notorious foodborne pathogen *Salmonella Typhimurium*.

There have been multiple genome-scale metabolic models constructed for *S. typhimurium* thus far. One of the starting metabolic reconstructions (MRs), *i*RR1083, was composed of 1083 genes, 1087 network reactions, and 744 unique metabolites (Raghunathan and others 2009). Following this, the BRecon model furthered the depth and accuracy of the previous model. This model was composed of 1222 genes, 2108 network reactions, and 1084 unique metabolites (Thiele and others 2011). The 3rd published model, named as iMA945, was constructed from previous *Escherichia coli (E. coli)* models, such as iAF1260, using homology and other bioinformatics criteria. This model contained 945 genes, 1964 network reactions, and 1036 unique metabolites (AbuOun and others 2009). More recently, a consensus reconstruction was performed, where over 20 experts in *S. typhimurium* and systems biology collaborated to produce a more comprehensive model with more detail and accuracy than ever before. This published consensus model, known as STM_v1.0, encompasses 1270 genes, 2201 network reactions, and 1119 unique metabolites (Thiele and others 2011). Although these mentioned models are comprehensive representations of *S. typhimurium*'s metabolic network, the reactions for biofilm formation have not yet been included. Additionally, no systems-level approaches have been developed to study the biofilm formation of *S. typhimurium*. The primary goals of this work are to 1st extend the current metabolic model of *S. typhimurium* in MATLAB, to include certain associated reactions and metabolites that are correlated with biofilm formation, and to develop a systems-level approach to investigate the adjustment of intracellular metabolism that occurs during biofilm growth.

Methods

Original genome-scale model for *S. typhimurium*

The starting MR used in this work was a recently updated version of the Salmonella model, called as STM_v1.0, which was previously described in Thiele and others 2011. The version of STM_v1.0 has been extended to include additional information gathered over the years since its initial publication. This updated model, obtained directly through Ines Thiele's team by personal contact, was composed of 1271 total genes, 2546 total network reactions, and 1802 total metabolites prior to the extension performed in this study. STM_v1.0 is currently the most comprehensive genome-scale metabolic model for *S. typhimurium*, having integrated and/or built upon all preceding models. Significant renovations from previous models include accounting for the periplasm compartment between the cytoplasm and extracellular space, addition of virulence characteristics that are specific to Salmonella (such as O-antigen production, which is involved in ECA and mature LPS synthesis), incorporation of thermodynamic

information, and supplementation of widespread support data for reactions and their associated genes (Thiele and others 2011). STM_v1.0 was chosen as the initial model in this work due to its renewed and comprehensive nature.

Extension of the metabolic model of *S. typhimurium*

In order to explore the intracellular metabolism of *S. typhimurium* during the biofilm formation, the extension of the starting Salmonella metabolic model was required. Reactions and metabolites associated with the direct formation of biofilm were not present in STM_v.10, therefore, their review, understanding, and addition to the current model were necessary. Initially, a literature review was conducted to better understand the cellular metabolism of *S. typhimurium* under biofilm growth conditions. The following question needed to be answered: What essential genes are involved during the formation of the extracellular biofilm matrix? Determining the reactions that these genes encode for, and the metabolites directly involved in these reactions, was also an essential aspect of the literature review.

A precedent genetic analysis of biofilm formation in Salmonella was the primary starting point for the investigation of essential biofilm components (Solano and others 2002). This study determined that colanic acid, LPS, ECA, and cellulose are essential components of a fully expressed biofilm when in nutrient rich conditions such as lysogeny broth (LB) medium (*in vitro*) or animal cell tissue (*in vivo*) (Solano and others 2002). However, variations in growth media revealed that biofilm composition and regulation are highly dependent on environmental conditions (Solano and others 2002). This finding has been strongly backed by a variety of other studies (Romling 2005; Kolter and Greenberg 2006; Kim and others 2013). Cellulose was determined as a predominant biofilm component, and largely comprises the EPSs that form the biofilm matrix (Solano and others 2002; de Rezende and others 2005). Solano established that cellulose is the only contributing component of the biofilm formed in nutrient deficient media, such as on an abiotic surface (Solano and others 2002). These results were also consistent with multiple other studies (Prouty and Gunn 2003; Jonas and others 2007). Colanic acid is also not required for the biofilm formation of Salmonella on abiotic surfaces (Gibson 2000; Prouty and Gunn 2003), and the production of colanic acid hinders virulence and successful infection (Mouslim and others 2004). To concentrate on biofilm formation in a virulent setting, as well as focus efforts toward growth in deficient media, colonic acid was excluded in this model extension.

Due to its heavily contributing nature in biofilm formation, cellulose was a primary focus throughout this work. There are 2 operons, *bcsABZD* and *bcsEFG*, which are required for cellulose biosynthesis in Salmonella (Solano and others 2002). Of these genes, *bcsA* is the most essential as it codes for the cellulose synthase catalytic subunit that utilizes uridine-diphosphate (UDP) glucose, a nucleotide sugar molecule, to form and extend the polysaccharide that is cellulose (Kanehisa and Goto 2000; Kanehisa and others 2015). The production and metabolic biosynthesis pathways of both LPS and ECA were also key focuses in this work. The LPS biosynthesis pathway begins with UDP-N-acetyl-D-glucosamine, and after several enzymatic steps, ultimately yields a complete LPS molecule. LPS later reacts with the end product of ECA biosynthesis, *via* an O-antigen translocase enzyme coded for by *wzxE* (STM3926), to form mature LPS (Kanehisa and Goto 2000; Solano and others 2002; Kanehisa and others 2015). This mature LPS is a primary contributor to biofilm formation in nutrient rich conditions.

The genome-scale MR for *S. typhimurium*, STM_v1.0 (Solano and others 2002), was extended to include the necessary reactions for biofilm formation in a virulent state. In order to extend the current Salmonella model to include cellulose production, cellulose itself was added into the model by creating exchange reactions for 2 separate cellulose metabolites. These necessary exchange reactions sanction the uptake of the cellulose metabolites, which allows for their use in subsequent reactions throughout the model. The 1st metabolite (that is, Cellulose_n) was an initial cellulose molecule, and the 2nd (that is, Cellulose_{n+1}) was an extended chain of cellulose after the addition of glucose from UDP-glucose, which takes place *via* cellulose synthase during the cellulose formation reaction shown in Eq. (1) (Kanehisa and Goto 2000; Kanehisa and others 2015):

$$\text{UDP} - \text{glucose} + \text{Cellulose}_n \Rightarrow \text{UDP} + \text{Cellulose}_{n+1} \quad (1)$$

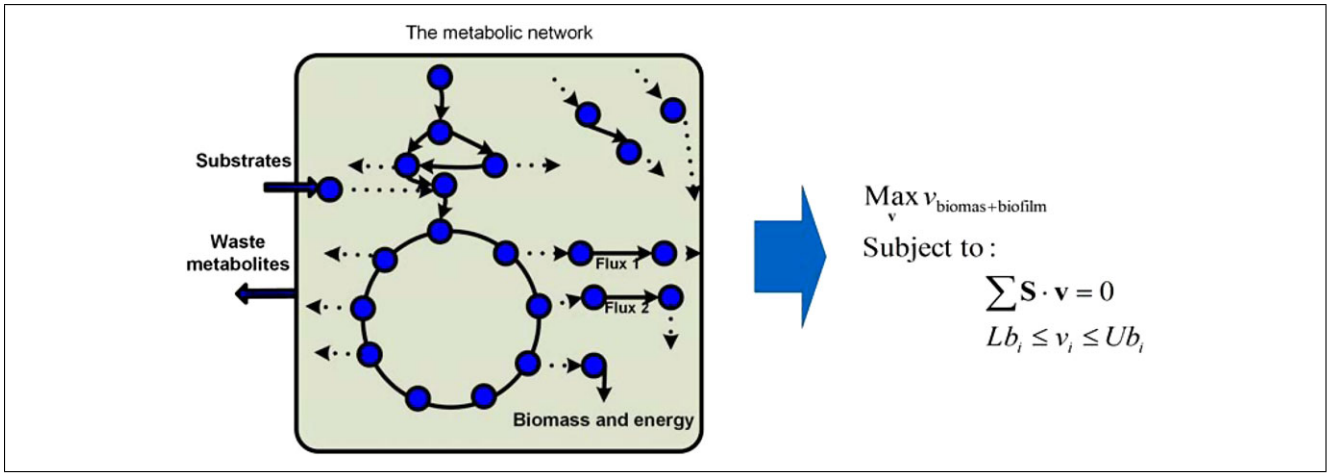

Figure 1–The genome-scale metabolic model is subjected to FBA with a defined objective function to quantify the biomass growth rate and the production rates of biofilm components. The environmental conditions are integrated in the modelby the upper and lower bounds of reaction fluxes, that is, Ub_i and Lb_i. In particular, the upper and lower bounds of those exchange reactions for extracellular metabolites/nutrients to mimic the rich and minimal medium conditions as suggested in Raghunathan and others 2009. Based on the stoichiometric and capacity constraints, an optimal flux distribution is calculated within the bounds of the allowable solution space to quantify possible maximum objective function, $v_{\text{biomass+biofilm}}$.

All of the reactions associated with the biosynthesis of LPS, ECA, and the ultimately mature combination of LPS and ECA (represented by LPS-ECA in the following text) were already present in STM_v1.0; therefore, their addition was not necessary. However, to incorporate them into a complete biofilm growth reaction, the end-product reactions of these metabolites were taken into account. The added cellulose synthase reaction, and the culminating reactions for LPS and ECA, and the original biomass growth reaction were used to construct the biofilm plus biomass growth reaction displayed in Eq. (2). This overall biofilm, which is represented by the combination of cellulose, ECA, and LPS, plus biomass growth reaction, was also introduced into to the STM_v1.0 model. This extended model was referred to as STM_v2.0 throughout experimentation. In addition to the reactions shown in STM_v1.0 model, STM_v2.0 included exchange reactions for the new cellulose metabolites, the cellulose formation reaction, and a biofilm formation reaction that castoff of the final reactions in the LPS and ECA biosynthesis pathways.

$$pct_{\text{biomass}} \times \mu_{\text{biomass}} + (1 - pct_{\text{biomass}})\,[pct_{\text{cellulose}} \times v_{\text{cellulose}} + (1 - pct_{\text{cellulose}}) \times v_{\text{LPS-ECA}}] \rightarrow \text{Environment} \quad (2)$$

where μ_{biomass} refers to the cellular mass growth rate (h^{-1}), $v_{\text{cellulose}}$ refers to the production rate of cellulose ($mmol \cdot gDW^{-1}h^{-1}$), and $v_{\text{LPS-ECA}}$ refers to the production rate of LPS-ECA ($mmol \cdot gDW^{-1}h^{-1}$). The coefficient pct_{biomass} represents the mass percentage of the biomass in the biomass and biofilm mixture. pct_{biomass} was initially set to 0.35 that indicates 35% of the biomass-biofilm mixture is cellular biomass. This expected pct_{biomass} is based on the collected data and concluding results from multiple studies on biofilm formation (Jahn 1998; Laspidou and Rittmann 2004; Velten and others 2007). pct_{biomass} was further varied in FBA to study the scenarios in which the ratio of cellular biomass to biofilm changes during biofilm growth. $pct_{\text{cellulose}}$ is a factor that indicates the mass percentage of cellulose in the extracellular biofilm matrix (that is, the mixture of cellulose and LPS-ECA). A large $pct_{\text{cellulose}}$ indicates that cellulose is the primary component in the biofilm matrix. The reaction flux of Eq. (2) is represented as $v_{\text{biomass+biofilm}}$ for FBA.

Flux balance analysis to quantify the biofilm formation of *S. typhimurium*

FBA is extensively used in the field of systems biology to better understand the functions of biochemical metabolic networks,

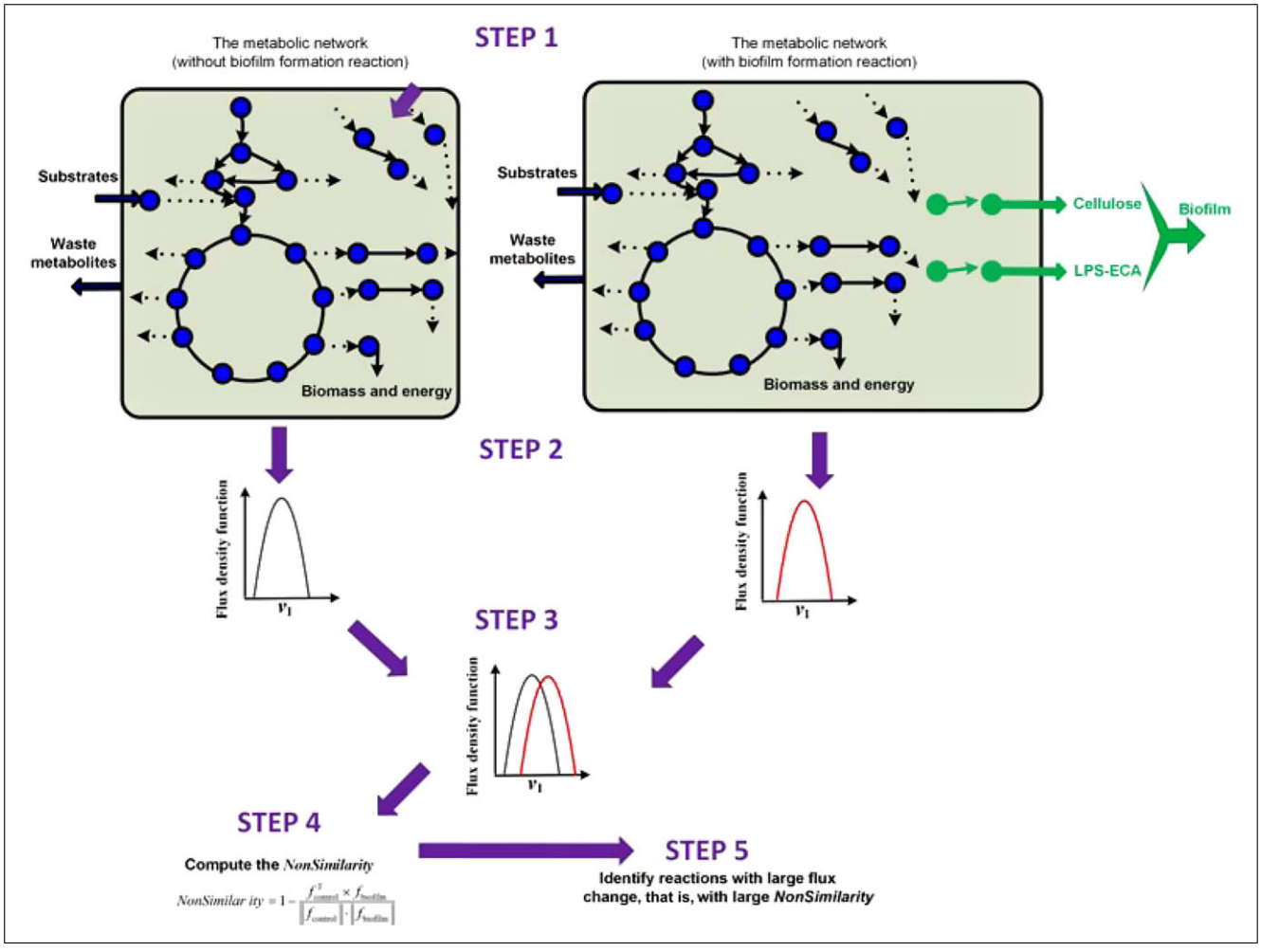

Figure 2–Determining the changes of intracellular metabolic fluxes during biofilm formation. Step 1 involves setting up the metabolic model to function based on the appropriate conditions. The 1st condition was without biofilm formation (the control), and the 2nd was with biofilm formation. Step 2 is to run an ACHR algorithm to generate predicted flux distributions of every metabolic reaction for each of the 2 model simulations. Step 3 is to compare the changes in flux distributions between the 2 conditions, and determine the magnitude of flux variation, which involves both steps 4 and 5.

Table 1–Simulation results of biomass growth and biofilm formation in a minimal medium.

Simulation conditions	Cellular mass growth rate (h^{-1})	Production rate of LPS-ECA ($mmol \cdot gDW^{-1}h^{-1}$)	Production rate of cellulose ($mmol \cdot gDW^{-1}h^{-1}$)
Planktonic condition (that is, no biofilm formation)	1.0053	0	0
Matured biofilm (100% cellulose mass)	0.6238	0	1.1584

$pct_{biomass}$ was set to 0.35, and $pct_{cellulose}$ was equal to 1.0.

because it allows for the quantifiable and dynamic interpretation of metabolic physiology (Varma and Palsson 1994; Raman and Chandra 2009). On the basis of the extended Salmonella model, FBA was implemented to quantify biomass growth rate and the production rates of biofilm components cellulose and LPS-ECA in the nutrient conditions the model is subjected to. Reaction fluxes are the net rates at which molecules flow through a metabolic pathway. Every reversible reaction in a pathway has a forward and reverse rate of reaction, and the combination of these rates equates to the reaction's overall flux. At a state of equilibrium, the total flux of a particular metabolite is zero. Individual reaction fluxes are regulated by enzymatic action throughout metabolic pathways, and this cellular regulation is essential for optimal functionality under fluctuating environmental conditions (Orth and others 2010). FBA is a calculation-based approach for analyzing the regulation of metabolic pathways throughout an organism's metabolic network. This mathematical approach has been a fundamental asset in the analysis of genome-scale MRs, metabolic engineering, and drug target identification (Raman and Chandra 2009).

In MATLAB, the genome-scale model has a stoichiometric matrix (**S**), which represents all of the metabolic reactions in the cellular network in correspondence with all of the unique metabolites. The size of the matrix is defined by the number of unique metabolites (m), represented in individual rows, and the number of metabolic reactions (n), represented in individual columns. Each reaction column contains the stoichiometric coefficients for every participating metabolite, positive for those produced, negative for those consumed, and zero for all metabolites that are not involved in the particular reaction. The metabolic flux of every reaction in the model is represented by the element in the vector (**v**). The basis of FBA revolves around satisfying the resulting system of mass balance equations at steady state. At steady state, the net fluxes of all metabolites should be zero, and therefore adhere to Eq. (3):

$$\mathbf{S} \times \mathbf{v} = 0 \tag{3}$$

The computational analysis that takes place during FBA solves for a vector **v** that satisfies Eq. (3). In STM_v2.0, there are far more network reactions than unique metabolites, parallel to most large-scale models, therefore, there exist multiple solutions for this system of equations. In order to combat this, model constraints are set to define a specific range of solutions. This does not directly narrow the results down to a singular solution; however, it defines an allowable solution space imposed by mass balance constraints in **S**, as well as capacity constraints enforced by upper and lower bounds of reaction fluxes. Defining an objective reaction flux (named as the objective function in FBA) and focusing on the optimization of this particular reaction allow for FBA to identify a precise flux distribution, **v**.

To study the influence of biofilm formation on the metabolic network, Eq. (2) was defined as the objective function for FBA, and maximized through computational analysis. This constraint-based approach narrows down the possible solution space and

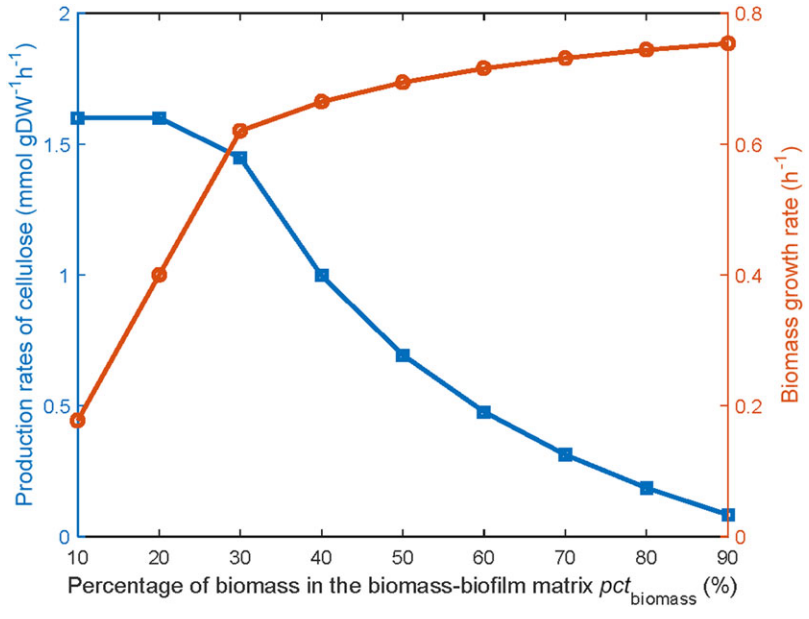

Figure 3–Simulation results for biomass growth rate and cellulose production rate based on a varying mass percentage of biomass in the biomass-biofilm matrix in the minimal medium.

Table 2–Simulation results of biomass growth and biofilm formation in a rich medium.

Simulation conditions	Cellular mass growth rate (h^{-1})	Production rate of LPS-ECA ($mmol \cdot gDW^{-1}h^{-1}$)	Production rate of cellulose ($mmol \cdot gDW^{-1}h^{-1}$)
Planktonic condition (that is, no biofilm formation)	2.6209	0	0
Matured biofilm	0.8675	0.1611	1.4500

$pct_{biomass}$ was set to 0.35, and $pct_{cellulose}$ was equal to 0.9.

optimizes biomass growth and the production rates of biofilm components LPS-ECA and cellulose, given a set of specific bounds and limitations, as illustrated in Figure 1.

Utilizing Eq. (2) as the objective function, multiple simulations of FBA were performed on the model. The 1st FBA simulation was performed in a nutrient deficient medium (that is, minimal medium). This simulation represents how the biomass and biofilm would grow on an abiotic surface, such as a medical device or metal surface in a food production facility. As previously stated, biofilm formation on an abiotic surface does not involve the production of LPS-ECA as the nutrients are simply not enough to properly fuel their formation (Solano and others 2002; Prouty and Gunn 2003; Jonas and others 2007). For this simulation, cellulose's mass fraction in the extracellular biofilm matrix $pct_{cellulose}$ was increased to 1.0 in order to block the production of LPS-ECA. This initial FBA simulation adhered to the assumed distribution of 35% biomass in the objective function, that is, $pct_{biomass}$ was set to 0.35 as discussed in the previous section. A simulation was further performed (under the same nutrient conditions) varying this biomass-biofilm distribution (that is, $pct_{biomass}$) to better understand how it influences overall growth and productions rates. For this purpose, the percentage of biomass in the biomass/biofilm composition $pct_{biomass}$ was varied from 0.1 to 0.9 in increments of 0.1. Understanding biofilm growth under these conditions is essential toward the fight against Salmonella infections through medical devices and food processing facilities.

To study the influence of environmental conditions, simulations were performed in a nutrient rich medium where both cellulose and LPS-ECA are contributing components to biofilm growth (Solano and others 2002). This simulation assumed that cellulose made up the majority of the EPS in the formed biofilm (Solano and others 2002; de Rezende and others 2005), therefore its mass fraction in the extracellular biofilm $pct_{cellulose}$ was set to 0.9. The influence of biofilm component compositions on the overall biomass growth rate was further analyzed. This simulation was performed by varying the percentages of cellulose in the biofilm reaction (that is, $pct_{cellulose}$) to better understand how the distribution of these components in biofilm formation affects the overall growth rate of the cell. In particular, $pct_{cellulose}$ was varied from 0.1 to 0.9 in increments of 0.1.

The change of the distributions of intracellular metabolic fluxes upon the biofilm formation

To determine the range and distribution of flux values for all reactions in the metabolic network, a Monte Carlo sampling approach was employed *via* an artificial centering hit-and-run (ACHR) algorithm. ACHR, which is provided through the COBRA toolbox (Becker and others 2007; Schellenberger and others 2011), is essentially an algorithm that randomly samples a valid solution point value within the defined constraints for, however, many iterations it is asked to complete (Kaufman and Smith 1998; Schellenberger and Palsson 2008). For these simulations, a total

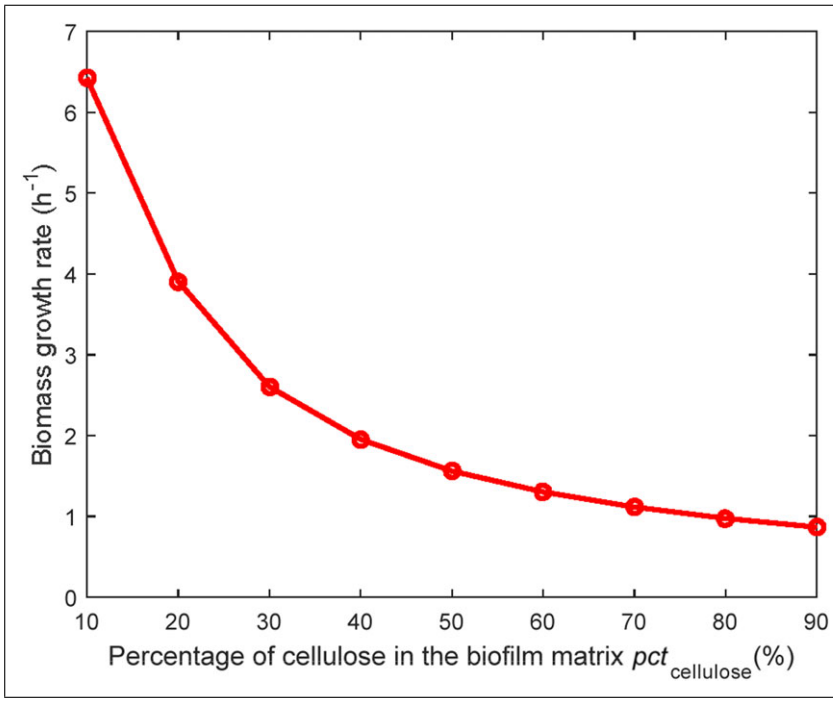

Figure 4–The biomass growth rate upon the change in the percentages of cellulose $pct_{cellulose}$ in the extracellular biofilm matrix.

of 100000 samples for each metabolic flux were used to make sure the sampling reaching was fully converged. This allows for an accurately defined flux distribution of each reaction in the entire metabolic network. The key here is not the flux distribution itself, but monitoring the changes or shifts in distributions under varying conditions. In this particular investigation, the sampling approach was used to define metabolic flux distributions for the entire model under the control condition without any biofilm formation, and then again for the entire model with the biofilm growth reaction taking place. The resulting flux distributions for the model with and without biofilm formation were then compared using a comparative analysis technique termed *NonSimilarity*, as described by Eq. (4).

$$NonSimilarity = 1 - \frac{f_{\text{control}}^{\text{T}} \times f_{\text{biofilm}}}{\| f_{\text{control}} \| \cdot \| f_{\text{biofilm}} \|} \quad (4)$$

where f_{control} and f_{biofilm} represent distributions of fluxes of simulations without and with biofilm formation, respectively. If f_{control} and f_{biofilm} are the same, the 2nd term in Eq. (4) is equal to 1, so that the *NonSimilarity* has a value of 0. On the other hand, if f_{control} and f_{biofilm} are orthogonal, *NonSimilarity* is equal to 1. Therefore, *NonSimilarity* is used to identify the metabolic reactions with a large flux change during the biofilm formation. The reactions with the largest metabolic flux changes indicate how *S. typhimurium* changes intracellular metabolism for biofilm formation. This overall process of metabolic simulation sampling, flux distribution generation, and comparative analysis is illustrated in Figure 2.

Results and Discussion

Biomass growth and biofilm formation in the minimal medium

Using the biofilm formation reaction as the objective function, FBA was conducted for the analysis of biomass growth rates, as well as the biofilm matrix component cellulose production rates, under both a planktonic condition and a matured biofilm condition in the minimal medium. As mentioned in the literature (Solano and others 2002; Prouty and Gunn 2003; de Rezende and others 2005; Jonas and others 2007), the production of LPS-ECA is not present in the Salmonella biofilm in a nutrient deficient medium. The simulation results shown in Table 1 represent how the biomass and biofilm grow on an abiotic surface, such as a medical device or metal surface in a food production facility. In this simulation, cellulose's contributing factor was increased to 1.0. As indicated in Table 1, the biomass growth rate was decreased from 1.0053 to 0.6238 h^{-1} after *S. typhimurium* forms biofilms. This is expected as bacteria are known to slow down biomass growth and save nutrients to produce extracellular biofilm matrix.

The initial FBA simulation adhered to the assumed distribution of 65% biofilm (represented by cellulose in this case as no LPS-ECA is produced in the minimal medium) and 35% biomass in the objective function (that is, pct_{biomass} equal to 0.35), however, the percentage of biofilm in the complex of the cellular biomass and biofilm may change over time during the biofilm formation process. More specifically, there should be less biofilm matrix formed during the early stages of overall biofilm formation. Therefore, the percentage of biomass pct_{biomass} was changed from 10% to 90% of the total biomass-biofilm mixture in a further simulation (under the same nutrient condition) to quantify the cellular growth rate in the minimal medium. For this simulation, the biomass factor, representing the percentage of biomass in the biomass-biofilm composition, was varied from 0.1 to 0.9 in increments of 0.1. The results of this simulation are summarized in Figure 3.

Figure 3 demonstrates that as the contribution of biomass increases in the biomass-biofilm mixture, the overall cellular growth rate increases as well. On the other hand, the overall production rates of biofilm formation component (that is, cellulose) decrease. Both results are consistent with predictions that growth rates and production rates maintain a direct relationship with component contribution. If there is less biomass involved, the growth rate of

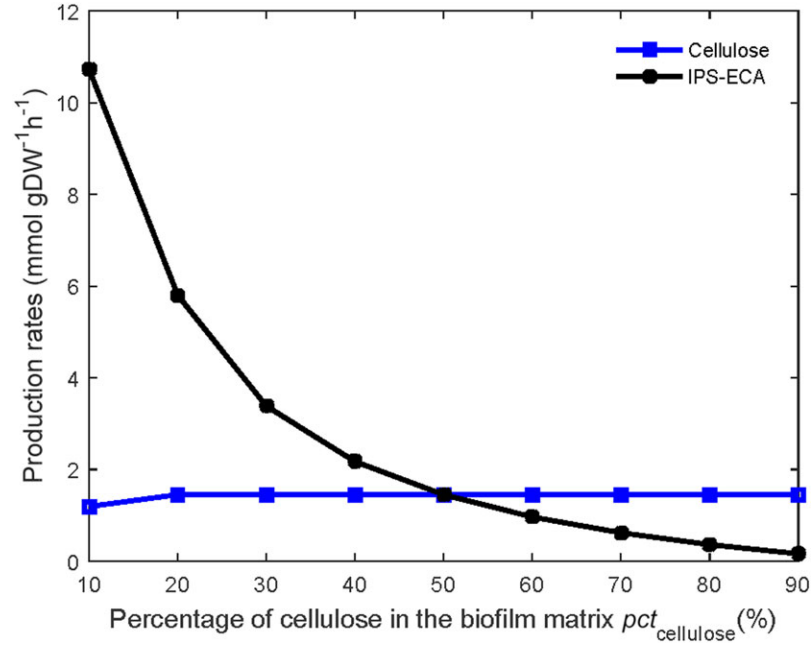

Figure 5–The production rates of LPS-ECA and cellulose upon the change in the percentages of cellulose $pct_{\text{cellulose}}$ in the extracellular biofilm matrix.

Table 3–Top 32 reactions with largest flux changes and *NonSimilarity* values larger than 0.8.

Reaction index number	Gene name(s)	Enzyme EC number(s)	Enzyme names	References indicating enzyme-biofilm relevance
1515	*mgsA*	EC:4.2.3.3	Methylglyoxal synthase	Lu and others 2014
1358	*gldA*	EC:1.1.1.6	Glycerol dehydrogenase	Lu and others 2014
215	*nagZ*	EC:3.2.1.52	β-N-acetylhexosaminidase	Nelson 2013
265	*ampD*	*	1,6-anhydro-N-acetylmuramyl-L-alanine amidase AmpD	Lappann and others 2010
78, 79, 80, 69	*fabZ; fabA*	EC:4.2.1.59; EC:5.3.3.14	3-Hydroxyacyl-[acyl-carrier-protein] dehydratase; trans-2-decenoyl-[acyl-carrier protein] isomerase	Singh and others 2009
95, 96, 97, 86, 89	*fabG*	EC:1.1.1.100	3-Oxoacyl-[acyl-carrier protein] reductase	Lai and Cronan 2004
107, 108, 98, 101, 1338	*fabF; fabB*	EC:2.3.1.179; EC:2.3.1.41	3-Oxoacyl-[acyl-carrier-protein] synthase II; 3-oxoacyl-[acyl-carrier-protein] synthase I	Lai and Cronan 2004
121	*gutQ*	EC:5.3.1.13	Arabinose 5-phosphate isomerase	Herzberg and others 2005
1348	*kdsB*	EC:2.7.7.38	3-Deoxy-manno-octulosonate cytidylyltransferase (CMP-KDO synthetase)	Strohmaier and others 1995
1349	*kdsC*	EC:3.1.3.45	3-Deoxy-D-manno-octulosonate 8-phosphate phosphatase (KDO 8-P phosphatase)	Martorana and others 2011
1350	*kdsA*	EC:2.5.1.55	2-Dehydro-3-deoxyphosphooctonate aldolase (KDO 8-P synthase)	Yeom and others 2012
1374	*lpxB*	EC:2.4.1.182	Lipid-A-disaccharide synthase	Albers and others 2007
1547, 1548	*kdtA*	EC:2.4.99.12, EC:2.4.99.13, EC:2.4.99.14, EC:2.4.99.15	3-Deoxy-D-manno-octulosonic-acid transferase	Tan and Darby 2006
2034	*lpxK*	EC:2.7.1.130	Tetraacyldisaccharide 4′-kinase	Youngjae and Jubee 2014
2101	*lpxD*	EC:2.3.1.191	UDP-3-O-[3-hydroxymyristoyl] glucosamine N-acyltransferase	Albers and others 2007
2108	*lpxA; acpP*	EC:2.3.1.129; *	UDP-N-acetylglucosamine acyltransferase; acyl carrier protein	Albers and others 2007; Mitev and others 2009
2133	*lpxC*	EC:3.5.1.108	UDP-3-O-[3-hydroxymyristoyl] N-acetylglucosamine deacetylase	Albers and others 2007
2159	*lpxH*	EC:3.6.1.54	UDP-2,3-diacylglucosamine hydrolase	Babinski and others 2002
608	*fabI*	EC:1.3.1.9, EC:1.3.1.10	Enoyl-[acyl-carrier protein] reductase I	Lai and Cronan 2004
1360	*No gene associated*	*		

Note:
* Indicates that no relevant data were acquired.
$pct_{biomass}$ was set to 0.35, and $pct_{cellulose}$ was equal to 1.0 in FBA simulations.

such will decrease. The same is true for biofilm formation and the production rates of its constituents.

Biomass growth and biofilm formation in the rich medium

To study the influence of environmental conditions on biomass and biofilm formation, the 2nd simulation performed was to access the influence of biofilm formation on the growth rate of cellular mass in a nutrient rich medium. In the nutrient rich medium, both cellulose and LPS-ECA are contributing components to biofilm growth (Solano and others 2002). This simulation assumed that cellulose made up the majority of the EPS in the formed biofilm (Solano and others 2002; de Rezende and others 2005), therefore its mass fraction $pct_{cellulose}$ in the extracellular biofilm was set to 90%. The influence of $pct_{cellulose}$ on the biofilm formation was further invested in the next section. In the simulation, the biomass fraction in the biomass-biofilm mixture was kept the same as the one used for the minimal medium, that is, $pct_{biomass}$ was set to 0.35. The resulting cellular growth rate and biofilm component production rates are outlined in Table 2. The overall growth rate of cellular biomass and the cellulose production rates are greater in the rich media simulation when compared to the minimal media. This indicates that the added nutrients in the rich medium further stimulate the growth of pathogens and thus the production of important biofilm components such as cellulose and LPS-ECA (Solano and others 2002; Prouty and Gunn 2003; de Rezende and others 2005; Jonas and others 2007).

The influence of biofilm component compositions on the overall biomass growth rate was further analyzed by varying the percentages of cellulose $pct_{cellulose}$ in the biofilm reaction. The results of this simulation are illustrated in Figure 4 and 5. It is interesting to see in Figure 4 that the biomass growth rate decreases as the mass fraction of cellulose in the extracellular biofilm matrix increases. While no direct experimental data have been found in the literature to prove this, one potential explanation is that the increasing cellulose in the biofilm inhibits bacterial motility and thus prevents the bacteria from obtaining new nutrients for growth. A high biomass growth rate is associated with a low $pct_{cellulos}$. This may not happen in reality, as cellulose generally occupies a large portion of the biofilm matrix.Figure 5 shows that the production rates of LPS-ECA and cellulose decrease and increase, respectively, upon the increase of the mass fraction of cellulose in the extracellular biofilm matrix.The results shown in Figure 4 and 5 provide hypotheses for further experiment investigation.

Variation of intracellular metabolic fluxes during biofilm formation

In order to validate the modeling approach presented in this work, the reactions important for the biofilm formation of *S. typhimurium* were 1st identified as those with large metabolic flux change upon the biofilm formation. These reactions were then compared with experimental data in this section. Specifically, an ACHR sampling approach was used to define metabolic flux distributions for the entire model under the control condition without any biofilm formation, and then again for the entire model with the biofilm growth reaction taking place. The FBA was performed for the minimal medium in the ACHR sampling approach, with $pct_{biomass}$ and $pct_{cellulose}$ set to 0.35 and 1.0, respectively. The resulting flux distributions for the model with and without biofilm formation were then compared using *NonSimilarity* defined in Eq. (4). The reactions that exhibited the largest flux changes, with a *NonSimilarity* value higher than 0.8 between the control and biofilm formation conditions, were deemed to have a significant impact during the growth of biofilm in *S. typhimurium*.The top 32 reactions and 22 associated genes based on this criterion are outlined in Table 3, referencing the STM_v2.0 reaction index numbers shown in the Supplementary Material 1, the KEGG gene names, and the KEGG enzyme (EC) numbers (Kanehisa and Goto 2000). Other reactions with lower *NonSimilarity* value can be provided upon request.

The comparative analysis of *NonSimilarity* was based on the difference in a reaction's flux distribution from the control condition of no biofilm formation to the biofilm formation condition. These reaction fluxes are compared based on the approach outlined in Figure 2. As an example, typical flux distribution profiles for 2 of the top reactions listed in Table 3 are shown in Figure 6.

In order to validate the reactions displayed in Table 3 for their important roles in regulating Salmonella biofilm formation, literature review on related genes were conducted and summarized in the following paragraphs. These 22 genes are mainly involved in the following KEGG pathways: LPS biosynthesis, fatty acid biosynthesis, fatty acid metabolism, biotin metabolism, propanoate metabolism, glycerolipid metabolism, amino sugar, and nucleotide sugar metabolism as shown in Figure 7. Based on the simulation results and supporting publications shown below, the reactions and genes listed in Table 3 are the most important with regard to the formation of biofilm in *S. typhimurium*. As such, these essential

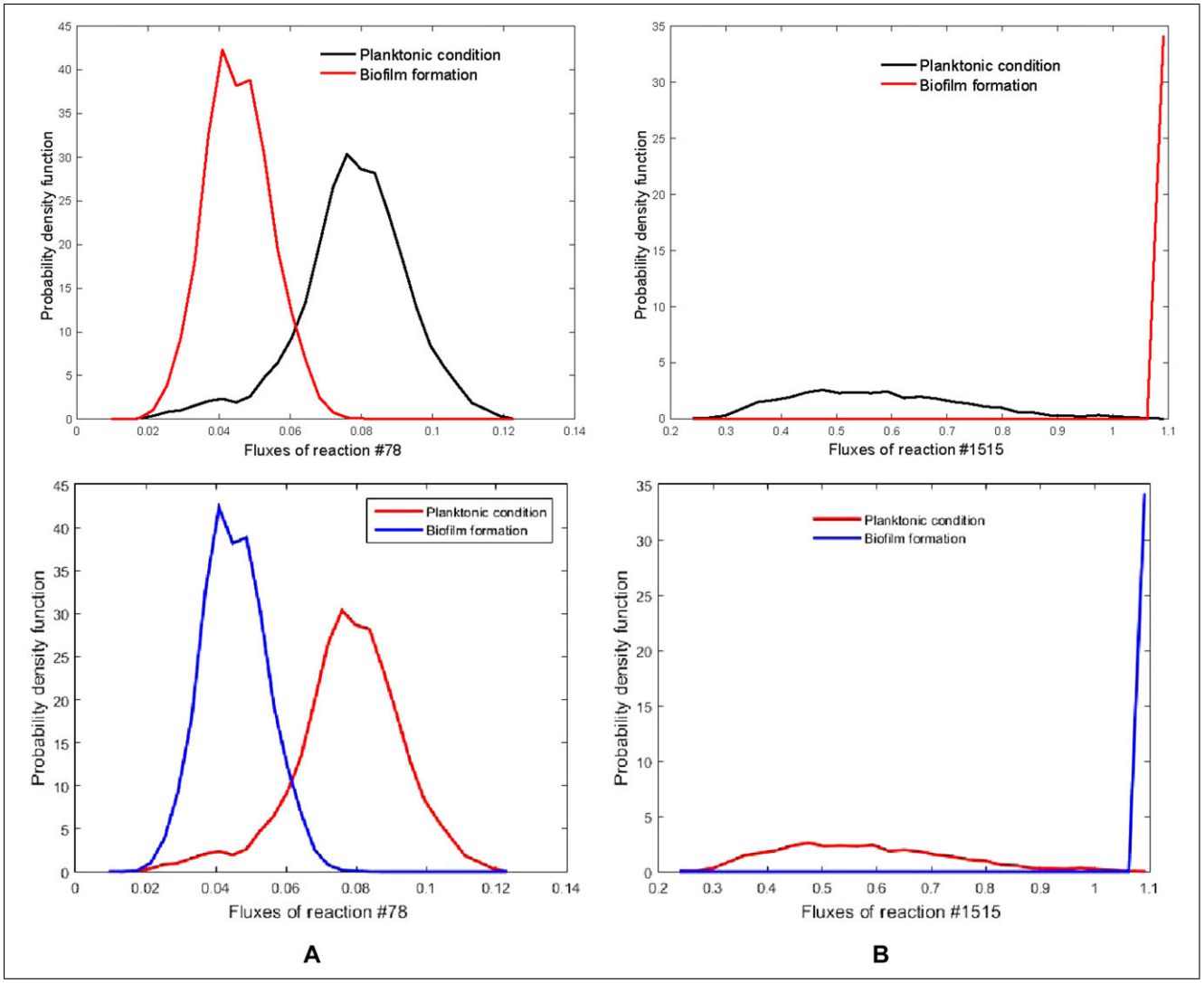

Figure 6–The flux distribution profiles of reaction #78 (A) and reaction #1515 (B) for both the planktonic condition and the biofilm formation condition. The genes associated with these 2 reactions can be found in Table 3.

genes should be the focus of further investigations into the biofilm formation of *S. typhimurium*.

Methylglyoxal synthase (*mgsA*) and glycerol dehydrogenase (*gldA*) play important roles in Salmonella growth due to their involvement in glycolytic pathways. *MgsA* may have an impact on glycolysis by controlling the formation of intermediates during the glycolytic conversion of dihydroxyacetone phosphate (DHAP) to pyruvate (Cooper and Anderson 1970; Hopper and Cooper 1971; Chakraborty and others 2014). *GldA* is a nicotinamide adenine dinucleotide oxidized form (NAD+) dependent enzyme that is involved in the transformation of intracellular dihydroxyacetone (DHA) to DHAP, a key glycolytic intermediate (Ribeiro

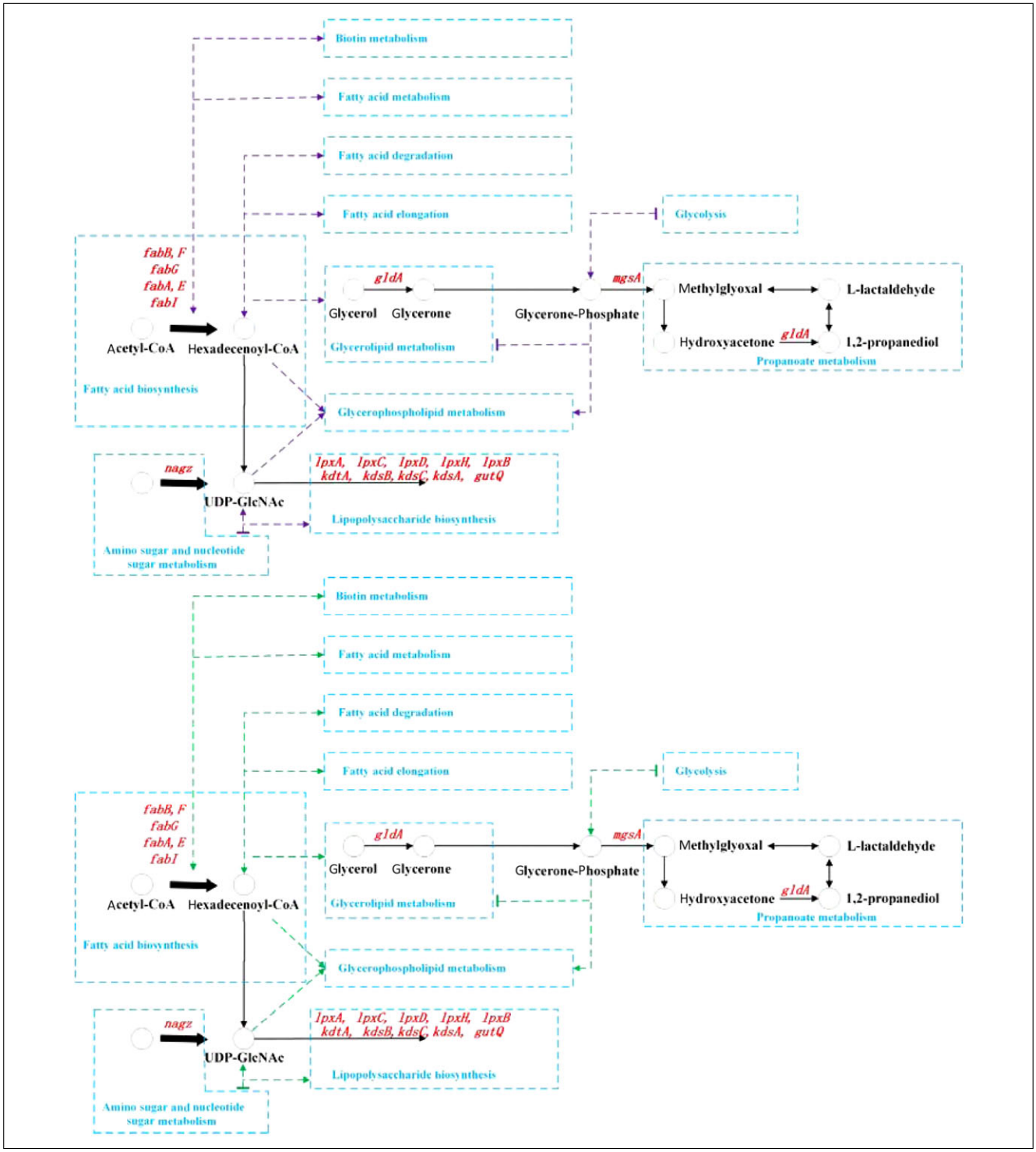

Figure 7–The distribution of the genes shown in Table 3 that are important to Salmonella biofilm formation in various metabolic pathways. In this figure, purple dash lines indicate connection between different KEGG pathways; blue lines/texts represent KEGG pathway names; black arrows represent metabolic reactions; the thick black arrow stands for a cascade of reactions but intermediate products are not shown; black circles and texts represent molecules; and red texts show the related gene names. The involvement of certain genes in the lipopolysaccharide biosynthesis is further illustrated in Figure 8.

and others 2013). *GldA* is also related with the maintenance of redox-balanced conditions during cell growth (Ribeiro and others 2013). Under stressful environmental conditions, Salmonella cells experience upregulation in *gldA* to compensate for induced changes in growth capabilities (Spory and others 2002; Shoae Hassani and others 2008). *MgsA* and *gldA* are also related with biofilm formation because the related molecule methylglyoxal is highly inhibitory to bacterial growth due to antibiofilm activities (Lu and others 2014). β-N-acetylhexosaminidase (*nagZ*), a putative depolymerase enzyme, displayed significant activity with regard to dissolve the extrapolymeric substance matrix associated with bacterial biofilms (Nelson 2013). *NagZ* is part of the peptidoglycan cell wall recycling pathway that can elevate the susceptivity of gram-negative bacteria to β-lactams (Mondon and others 2013). AmpD protein is also involved in the peptidoglycan cell wall recycling pathway in Salmonella, and *ampD* deficient mutants have shown significantly decreased cell growth and biofilm growth capabilities (Folkesson and others 2004).

FabA, *fabB*, *fabF*, *fabG*, *fabI*, and *fabZ* are all essential genes in fatty acid biosynthesis pathway, fatty acid metabolism, and biotin metabolism. Both *fabZ* and *fabA* encode acyl-carrier-protein (ACP) dehydratases that are directly involved in the fatty acid biosynthesis pathways of gram-negative bacteria (Heath and Rock 1996). This involvement in fatty acid synthesis is responsible for the redistribution of membrane fatty acids under survival conditions, allowing for continued existence (Singh and others 2009). *FabF* and *fabB* are β-ketoacyl-ACP synthases that catalyze the Claisen condensation reaction during the onset of fatty acid elongation. This vital role in fatty acid biosynthesis significantly affects cell viability (Lai and Cronan 2004). *FabG* is a β-ketoacyl-ACP reductase that catalyzes the redox reaction of β-ketoacyl-ACP to β-hydroxyacyl-ACP, which is a key step in the fatty acid elongation. Interference with *fabG* transcription blocks overall cell growth (Zhang and Cronan 1998). *FabI* is a nicotinamide adenine dinucleotide reduced form (NADH) dependent enoyl-ACP reductase that catalyzes the formation of acyl-ACP, which is the transferring step between the initial fatty acid elongation and the following elongation cycles (Lai and Cronan 2004). This cycle, involving the previous steps mentioned (with regard to *fabA*, *fabB*, *fabF*, *fabG*, and *fabZ*) is continually repeated until the acyl-ACP chain attains its required length to produce lipid A (Heath and Rock 1996; Lai and Cronan 2004). Lipid A, a bioactive component of LPS and ECA formation in the biofilm, is a fatty acid chain that is produced through fatty acid biosynthesis pathways (Raetz and Whitfield 2002).

Twelve genes are found by FBA to be involved in LPS biosynthesis pathway: *gutQ*, *kdsA*, *kdsC*, *kdsB*, *lpxA*, *lpxC*, *lpxD*, *lpxH*, *lpxB*, *lpxK*, and *kdtA*.The correlations among these genes are illustrated in Figure 8. LPS is the major component of the surface of gram-negative bacteria, and the close relationship between the presence of LPS and biofilm formation has been reported in *S. typhimurium* (Mireles and others 2001) and *E. coli* (Nakao and others 2012). 3-Deoxy-D-manno-oct-2-ulosonic acid (KDO) is an essential component of enterobacterial LPS (Strohmaier and others 1995), and interference in the KDO pathway leads to diminished LPS production and growth (Tan and Darby 2006). *GutQ* was discovered to play an important role in LPS biosynthesis (Meredith and Woodard 2005) and biofilm formation (Herzberg and others 2005), which is an arabinose 5-phosphate isomerase that converts ribulose 5-phosphate into arabinose 5-phosphate, an essential step in the initiation of the KDO pathway (Tan and Darby 2006). KDO 8-P synthase (*kdsA*) is also required for the biosynthesis of KDO (Zhou 2000). Under stressful conditions, *kdsA* is significantly upregulated by the cell in order to increase membrane rigidity (Yeom and others 2012). KDO-8-phosphate phosphatase (*kdsC*) catalyzes the hydrolysis of KDO-8-phosphate to KDO and inorganic phosphate in the KDO pathway, which is a critical step that precedes the transfer of KDO to LPS, therefore affecting mature LPS production and biofilm formation in later stages (Cipolla and others 2010; Martorana and others 2011). CMP-KDO synthetase (*kdsB*) catalyzes the activation of KDO and forms CMP-KDO, which is essential during the incorporation of KDO into lipid A (Strohmaier and others 1995), a critical process for biomass and biofilm growth (Helander and others 1992). KDO transferase (*kdtA*) is the key enzyme to catalyze KDO glycosylation of lipid A. In *kdtA*-deficient mutant, LPS lacks KDO and hence the size and viability of biofilms are significantly diminished (Tan and Darby 2006). The synthesis of lipid X, which is used later to synthesize lipid IVA and lipid A, from UDP-N-acetylglucosamine (UDP-GlcNAc), takes place through a number of enzymatic steps catalyzed by *lpxA*, *lpxC*, *lpxD*, and *lpxH* (Nakhamchik 2008). UDP-GlcNAc acyltransferase (*lpxA*) and UDP-3-O-(3-hydroxymyristoyl)-GlcN N-acyltransferase (*lpxD*) are primary acyl transferases involved in lipid A biosynthesis (Helander and others 1992; Albers and others 2007). Variation in *lpxA* expression is associated with cellular growth under varying

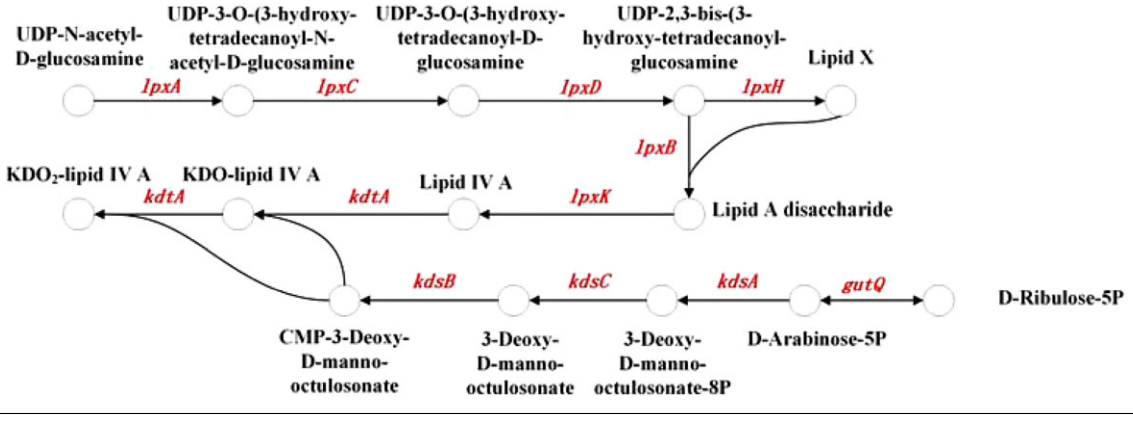

Figure 8–The involvement of genes *nagz*, *lpxA*, *lpxB*, *lpxC*, *lpxD*, *lpxH*, *lpxK*, *kdtA*, *kdsA*, *kdsB*, *kdsC*, and *gutQ* in the lipopolysaccharide biosynthesis. These reactions are from KEGG database.

environmental conditions (Albers and others 2007). *LpxA*, *lpxD,* and UDP-3-O-(3-hydroxymyristoyl)-GlcNAc deacetylase (*lpxC*) are abundantly expressed during intracellular growth and in biofilms of Legionella pneumophila, a gram-negative bacteria (Albers and others 2007). UDP-2,3-diacylglucosamine hydrolase (*lpxH*) is required for cell viability in gram-negative bacteria by the function of cleaving the pyrophosphate bond of the UDP-2,3-diacylglucosamine to produce lipid X (Babinski and others 2002). With lipid-A-disaccharide synthase (*lpxB*), 2 lipid X molecules are joined together to synthesize lipid A disaccharide (Albers and others 2007). Tetraacyldisaccharide 4'-kinase (*lpxK*) catalyzes the reaction to form lipid IVA from disaccharide lipid A (Garrett and others 1997; Trent 2001). Under acidic stress, Salmonella upregulates the expression of *lpxK* (Youngjae and Jubee 2014).*AcpP* is an acyl carrier protein that is essential for LPS biosynthesis and overall cell viability (Mitev and others 2009). FBA by another research has determined that *acpP* is an essential gene in the fatty acid biosynthesis pathway (Barat and others 2012).

Conclusions

This work presented an extended genome-scale metabolic model for *S. typhimurium*, which includes essential reactions for biofilm formation in a virulent state. This extended model, developed upon STM_v1.0 (Thiele and others 2011), is able to run high throughput *in silico* metabolic simulations for preliminary investigations into the biofilm formation of *S. typhimurium* in both rich and minimal media. FBA, Monte Carlo sampling, and the comparative analysis of flux distribution profiles based on *NonSimilarity* defined in Eq. (4) were the primary techniques employed to carry out these investigations. The results obtained indicate that the biomass-biofilm distribution of a cellular colony, the biofilm component composition, and the overall environmental conditions all influence the development of a matured biofilm in *S. typhimurium*. Additionally, the top 32 reactions, and associated genes, which have a significant impact during the growth of biofilm in *S. typhimurium*, were identified based on flux distribution variations during biofilm formation. This preliminary investigation of the adjustment of intracellular metabolism of *S. typhimurium* during biofilm formation will serve as a platform to conduct further studies such as the influence of gene knockouts on biomass growth and biofilm formation, as well as many other aspects of the biofilm formation of *S. typhimurium*.

Acknowledgments

We appreciate Ines Thiele and her team for kindly providing us with an up-to-date version of STM_v1.0 to begin our investigations from. This work was supported by the Army Research Office (W911NF-14-1-0279), and T.K.W. is the Biotechnology Endowed Professor at the Pennsylvania State Univ. There is no conflict of interest in this work.

References

AbuOun M, Suthers P, Jones G, Carter B, Saunders M, Maranas C, Woodward M, Anjum M. 2009. Genome scale reconstruction of a Salmonella metabolic model: comparison of similarity and differences with a commensal *Escherichia coli* strain. J Biol Chem 284:29480–8.

Albers U, Tiaden A, Spirig T, Al Alam D, Goyert S, Gangloff S, Hilbi H. 2007. Expression *of Legionella pneumophila* paralogous lipid A biosynthesis genes under different growth conditions. Microbiology 153:3817–29.

Babinski K, Kanjilal S, Raetz C. 2002. Accumulation of the lipid A precursor UDP-2,3-diacylglucosamine in an *Escherichia coli* mutant lacking the lpxh gene. J Biol Chem 277:25947–56.

Barat S, Steeb B, Maze A, Bumann D. 2012. Extensive in vivo resilience of persistent Salmonella. PLoS One 7:e42007.

Becker S, Feist A, Mo M, Hannum G, Palsson B, Herrgard M. 2007. Quantitative prediction of cellular metabolism with constraint-based models: the COBRA toolbox. Nat Protoc 2:727–38.

Beloin C, Ghigo J. 2005. Finding gene-expression patterns in bacterial biofilms. Trends Microbiol 13:16–9.

Björkman J, Hughes D, Andersson D. 1998. Virulence of antibiotic-resistant *Salmonella typhimurium*. Proc Natl Acad Sci 95:3949–53.

Bower C. 1999. Resistance responses of microorganisms in food environments. Intl J Food Microbiol 50:33–44.

Butcher E, Berg E, Kunkel E. 2004. Systems biology in drug discovery. Nat Biotechnol 22:1253–9.

Chakraborty S, Karmakar K, Chakravortty D. 2014. Cells producing their own nemesis: understanding methylglyoxal metabolism. IUBMB Life 66:667–78.

Chen J, Gomez JA, Höffner K, Phalak P, Barton PI, Henson MA. 2016. Spatiotemporal modeling of microbial metabolism. BMC Syst Biol 10:21.

Cipolla L, Gabrielli L, Bini D, Russo L, Shaikh N. 2010. Kdo: a critical monosaccharide for bacteria viability. Nat Prod Rep 27(11):1618–29.

Cooper R, Anderson A. 1970. The formation and catabolism of methylglyoxal during glycolysis in *Escherichia coli*. FEBS Lett 11:273–6.

de Rezende C, Anriany Y, Carr L, Joseph S, Weiner R. 2005. Capsular polysaccharide surrounds smooth and rugose types of *Salmonella enterica* serovar Typhimurium DT104. Appl Environ Microbiol 71:7345–51.

Feist A, Herrgard M, Thiele I, Reed J, Palsson B. 2008. Reconstruction of biochemical networks in microorganisms. Nat Rev Microbiol 7:129–43.

Folkesson A, Eriksson S, Andersson M, Park J, Normark S. 2004. Components of the peptidoglycan-recycling pathway modulate invasion and intracellular survival of *Salmonella enterica* serovar Typhimurium. Cell Microbiol 7:147–55.

Fux CA, Costerton JW, Stewart PS, Stoodley P. 2005. Survival strategies of infectious biofilms. Trends Microbiol 13(1):34–40.

Garrett T, Kadrmas J, Raetz C. 1997. Identification of the gene encoding the *Escherichia coli* lipid A 4′-kinase: facile phosphorylation of endotoxin analogs with recombinant Lpxk. J Biol Chem 272:21855–64.

Gibson D. 2000. Salmonella enteritidis thin aggregative fimbriae and the extracellular matrix [PhD thesis]. Univ. of Victoria, Victoria, BC, Canada.

Heath R, Rock C. 1996. Roles of the faba and fabz β-hydroxyacyl-acyl carrier protein dehydratases in *Escherichia coli* fatty acid biosynthesis. J Biol Chem 271:27795–801.

Helander I, Hirvas L, Tuominen J, Vaara M. 1992. Preferential synthesis of heptaacyl lipopolysaccharide by the ssc permeability mutant of *Salmonella typhimurium*. Eur J Biochem 204:1101–6.

Herzberg M, Kaye I, Peti W, Wood T. 2005. YdgG (TqsA) controls biofilm formation in *Escherichia coli* K-12 through autoinducer 2 transport. J Bacteriol 188:587–98.

Hopper D, Cooper R. 1971. The regulation of *Escherichia coli* methylglyoxal synthase; a new control site in glycolysis?. FEBS Lett 13:213–6.

Jahn A. 1998. Cell biomass and exopolymer composition in sewer biofilms. Water Sci Technol 37:17–24.

Jayasinghe N, Franks A, Nevin KP, Mahadevan R. 2014. Metabolic modeling of spatial heterogeneity of biofilms in microbial fuel cells reveals substrate limitations in electrical current generation. Biotechnol J 9:1350–61.

Jonas K, Tomenius H, Kader A, Normark S, Römling U, Belova L, Melefors Ö. 2007. Roles of curli, cellulose and BapA in Salmonella biofilm morphology studied by atomic force microscopy. BMC Microbiol 7:70.

Jun W. 2006. Structure–function relationships of periplasmic membrane-derived oligosaccharides in Salmonella growth and virulence [PhD thesis]. Univ. of Maryland, College Park, MD, USA.

Kanehisa M, Goto S. 2000. KEGG: kyoto encyclopedia of genes and genomes. Nucleic Acids Res 28:27–30.

Kanehisa M, Sato Y, Kawashima M, Furumichi M, Tanabe M. 2015. KEGG as a reference resource for gene and protein annotation. Nucleic Acids Res 44:D457–62.

Kaufman D, Smith R. 1998. Direction choice for accelerated convergence in hit-and-run sampling. Oper Res 46:84–95.

Kell D, Potgieter M, Pretorius E. 2015. Individuality, phenotypic differentiation, dormancy and 'persistence' in culturable bacterial systems: commonalities shared by environmental, laboratory, and clinical microbiology. F1000Res 4:179.

Kim T, Sohn S, Kim Y, Kim W, Lee S. 2012. Recent advances in reconstruction and applications of genome-scale metabolic models. Curr Opin Biotechnol 23:617–23.

Kim Y, Schmidt B, Kidwai A, Jones M, Deatherage Kaiser B, Brewer H, Mitchell H, Palsson B, McDermott J, Heffron F, Smith R, Peterson S, Ansong C, Hyduke D, Metz T, Adkins J. 2013. Salmonella modulates metabolism during growth under conditions that induce expression of virulence genes. Mol BioSyst 9(6):1522–34

Kolter R, Greenberg E. 2006. Microbial sciences: the superficial life of microbes. Nature 441:300–2.

Lai C, Cronan J. 2004. Isolation and characterization of β-ketoacyl-acyl carrier protein reductase (Fabg) mutants of *Escherichia coli* and *Salmonella enterica* serovar Typhimurium. J Bacteriol 186:1869–78.

Lappann M, Claus H, van Alen T, Harmsen M, Elias J, Molin S, Vogel U. 2010. A dual role of extracellular DNA during biofilm formation of *Neisseria meningitidis*. Mol Microbiol 75:1355–71.

Laspidou C, Rittmann B. 2004. Modeling the development of biofilm density including active bacteria, inert biomass, and extracellular polymeric substances. Water Res 38:3349–61.

Lu J, Turnbull L, Burke CM, Liu M, Carter DA, Schlothauer RC, Harry EJ. 2014. Manuka-type honeys can eradicate biofilms produced by *Staphylococcus aureus* strains with different biofilm-forming abilities. PeerJ 2:e326.

Mardinoglu A, Gatto F, Nielsen J. 2013. Genome-scale modeling of human metabolism—a systems biology approach. Biotechnol J 8:985–96.

Martorana A, Sperandeo P, Polissi A, Deho G. 2011. Complex transcriptional organization regulates an *Escherichia coli* locus implicated in lipopolysaccharide biogenesis. Res Microbiol 162:470–82.

Mazumdar V, Amar S, Segrè D. 2013. Metabolic proximity in the order of colonization of a microbial community. PLoS One 8:e77617.

Mead P, Slutsker L, Dietz V, McCaig L, Bresee J, Shapiro C, Griffin P, Tauxe R. 1999. Food-related illness and death in the United States. Emerg Infect Dis 5:607–25.

Meredith T, Woodard R. 2005. Identification of GutQ from *Escherichia coli* as a D-arabinose 5-phosphate isomerase. J Bacteriol 187:6936–42.

Mireles JR, Toguchi A, Harshey RM. 2001. *Salmonella enterica* serovar typhimurium swarming mutants with altered biofilm-forming abilities: surfactin inhibits biofilm formation. J Bacteriol 183(20):5848–54.
Mitev G, Mellbye B, Iversen P, Geller B. 2009. Inhibition of intracellular growth of *Salmonella enterica* serovar Typhimurium in tissue culture by antisense peptide-phosphorodiamidate morpholino oligomer. Antimicrob Agents Chemother 53:3700–4.
Mondon M, Hur S, Vadlamani G, Rodrigues P, Tsybina P, Oliver A, Mark B, Vocadlo D, Bleriot Y. 2013. Selective trihydroxyazepane NagZ inhibitors increase sensitivity of *Pseudomonas aeruginosa* to β-lactams. Chem Commun 49(93):10983–5.
Mouslim C, Delgado M, Groisman E. 2004. Activation of the Rcsc/Yojn/Rcsb phosphorelay system attenuates Salmonella virulence. Mol Microbiol 54:386–95.
Nakao R, Ramstedt M, Wai SN, Uhlin BE. 2012. Enhanced biofilm formation by *Escherichia coli* LPS mutants defective in Hep biosynthesis. PLoS One 7(12):e51241.
Nakhamchik A. 2008. Characterization of polysaccharide biosynthesis, structure and regulation in *Vibrio vulnificus* [PhD thesis]. Univ. of Toronto, Toronto, ON, Canada.
Nelson D. 2013. Rapid dispersion of polymicrobial wound biofilms with depolymerase enzymes. College Park, Md.: Univ. of Maryland.
Orth J, Thiele I, Palsson B. 2010. What is flux balance analysis?. Nat Biotechnol 28:245–8.
Price N, Papin J, Schilling C, Palsson B. 2003. Genome-scale microbial in silico models: the constraints-based approach. Trends Biotechnol 21:162–9.
Prouty A, Gunn J. 2003. Comparative analysis of *Salmonella enterica* serovar Typhimurium biofilm formation on gallstones and on glass. Infect Immun 71:7154–8.
Raetz CR, Whitfield C. 2002. Lipopolysaccharide endotoxins. Annu Rev Biochem 71:635–700.
Raghunathan A, Reed J, Shin S, Palsson B, Daefler S. 2009. Constraint-based analysis of metabolic capacity of *Salmonella typhimurium* during host–pathogen interaction. BMC Syst Biol 3:38.
Raman K, Chandra N. 2009. Flux balance analysis of biological systems: applications and challenges. Brief Bioinform 10:435–49.
Ribeiro C, Sobral M, Tanaka C, Dallagassa C, Picheth G, Rego F, Alberton D, Huergo L, Pedrosa F, Souza E, Fadel-Picheth C. 2013. Proteins differentially expressed by Shiga toxin-producing *Escherichia coli* strain M03 due to the biliar salt sodium deoxycholate. Genet Mol Res 12:4909–17.
Romling U. 2005. Characterization of the rdar morphotype, a multicellular behaviour in Enterobacteriaceae. Cell Mol Life Sci 62:1234–46.
Romling U, Sierralta W, Eriksson K, Normark S. 1998. Multicellular and aggregative behaviour of *Salmonella typhimurium* strains is controlled by mutations in the agfD promoter. Mol Microbiol 28:249–64.
Schellenberger J, Palsson B. 2008. Use of randomized sampling for analysis of metabolic networks. J Biol Chem 284:5457–61.
Schellenberger J, Que R, Fleming R, Thiele I, Orth J, Feist A, Zielinski D, Bordbar A, Lewis N, Rahmanian S, Kang J, Hyduke D, Palsson B. 2011. Quantitative prediction of cellular metabolism with constraint-based models: the COBRA toolbox V2.0. Nat Protoc 6:1290–307.
Shoae Hassani A, Malekzadeh F, Amirmozafari N, Hamdi K, Ordouzadeh N, Ghaemi A. 2008. Phage shock protein G, a novel ethanol-induced stress protein in *Salmonella typhimurium*. Curr Microbiol 58:239–44.
Sigurdsson G, Fleming RM, Heinken A, Thiele I. 2012. A systems biology approach to drug targets in *Pseudomonas aeruginosa* biofilm. PLoS One 7:e34337.
Singh J, Khalichi P, Cvitkovitch D, Santerre J. 2009. Composite resin degradation products from BisGMA monomer modulate the expression of genes associated with biofilm formation and other virulence factors in *Streptococcus mutans*. J Biomed Mater Res A 88A:551–60.
Solano C, Garcia B, Valle J, Berasain C, Ghigo J, Gamazo C, Lasa I. 2002. Genetic analysis of *Salmonella enteritidis* biofilm formation: critical role of cellulose. Mol Microbiol 43:793–808.
Spory A, Bosserhoff A, von Rhein C, Goebel W, Ludwig A. 2002. Differential regulation of multiple proteins of *Escherichia coli* and *Salmonella enterica* serovar Typhimurium by the transcriptional regulator SlyA. J Bacteriol 184:3549–59.
Stepanović S, Cirkovic I, Ranin L, Svabic-Vlahovic M. 2004. Biofilm formation by *Salmonella spp.* and *Listeria monocytogenes* on plastic surface. Lett Appl Microbiol 38:428–32.
Stoodley P, Sauer K, Davies D, Costerton J. 2002. Biofilms as complex differentiated communities. Annu Rev Microbiol 56:187–209.
Strohmaier H, Remler P, Renner W, Hogenauer G. 1995. Expression of genes KdsA and KdsB involved in 3-deoxy-D-manno-octulosonic acid metabolism and biosynthesis of enterobacterial lipopolysaccharide is growth phase regulated primarily at the transcriptional level in *Escherichia coli* K-12. J Bacteriol 177(15):4488–500.
Tan L, Darby C. 2006. Yersinia pestis YrbH is a multifunctional protein required for both 3-deoxy-D-manno-oct-2-ulosonic acid biosynthesis and biofilm formation. Mol Microbiol 61:861–70.
Thiele I, Hyduke D, Steeb B, Fankam G, Allen D, Bazzani S, Charusanti P, Chen F, Fleming R, Hsiung C, Keersmaecker S, Liao Y, Marchal K, Mo M, Özdemir E, Raghunathan A, Reed J, Shin S, Sigurbjörnsdòttir S, Steinmann J, Sudarsan S, Swainston N, Thijs I, Zengler K, Palsson B, Adkins J, Bumann D. 2011. A community effort towards a knowledge-base and mathematical model of the human pathogen Salmonella Typhimurium LT2. BMC Syst Biol 5:8.
Trent M. 2001. Accumulation of a polyisoprene-linked amino sugar in polymyxin-resistant *Salmonella typhimurium* and *Escherichia coli*. Structural characterization and transfer to lipid A in the periplasm. J Biol Chem 276:43132–44.
Varma A, Palsson B. 1994. Metabolic flux balancing: basic concepts, scientific and practical use. Bio/Technology 12:994–8.
Velten S, Hammes F, Boller M, Egli T. 2007. Rapid and direct estimation of active biomass on granular activated carbon through adenosine tri-phosphate (ATP) determination. Water Res 41:1973–83.
Vital-Lopez FG, Reifman J, Wallqvist A. 2015. Biofilm formation mechanisms of *Pseudomonas aeruginosa* predicted via genome-scale kinetic models of bacterial metabolism. PLoS Comput Biol 11(10):e1004452.
Xu Z, Fang X, Wood TK, Huang ZA. 2013. Systems-level approach for investigating *Pseudomonas aeruginosa* biofilm formation. PLoS One 8:e57050.
Xu Z, Islam S, Wood TK, Huang Z. 2015. An integrated modeling and experimental approach to study the influence of environmental nutrients on biofilm formation of *Pseudomonas aeruginosa*. BioMed Res Intl 506782:1–12.
Yeom J, Lee Y, Park W. 2012. Effects of non-ionic solute stresses on biofilm formation and lipopolysaccharide production in *Escherichia coli* O157:H7. Res Microbiol 163: 258–67.
Youngjae C, Juhee A. 2014. Physiological and molecular responses of antibiotic-resistant *Salmonella enterica* serovar Typhimurium to acid stress. Afr J Microbiol Res 8: 578–89.
Zhang Y, Cronan J. 1998. Transcriptional analysis of essential genes of the *Escherichia coli* fatty acid biosynthesis gene cluster by functional replacement with the analogous *Salmonella typhimurium* gene cluster. J Bacteriol 180(13):3295–303.
Zhou Z. 2000. High-resolution NMR spectroscopy of lipid A molecules containing 4-amino-4-deoxy-L-arabinose and phosphoethanolamine substituents. Different attachment sites on lipid A molecules from NH4VO3-treated *Escherichia coli* versus kdsA mutants of *Salmonella typhimurium*. J Biol Chem 275:13542–51.

Supporting Information

Additional Supporting Information may be found in the online version of this article at the publisher's website:

Supplementary Material 1. The extended genome-scale model of *S. typhimurium*.